CISTER
Research Centre in
Real-Time & Embedded
Computing Systems

Conference Paper

Characterization and Modeling of the Bicycle-Antenna System for the 2.4GHz ISM Band

Luís Pinto
Pedro Miguel Santos
Luís Almeida
Ana Aguiar

CISTER-TR-190615

Characterization and Modeling of the Bicycle-Antenna System for the 2.4GHz ISM Band

Luís Pinto, Pedro Miguel Santos, Luís Almeida, Ana Aguiar

CISTER Research Centre

Polytechnic Institute of Porto (ISEP P.Porto)

Rua Dr. António Bernardino de Almeida, 431

4200-072 Porto

Portugal

Tel.: +351.22.8340509, Fax: +351.22.8321159

E-mail:

https://www.cister-labs.pt

Abstract

Vehicular communication is rapidly becoming a standard reality, and precise models are necessary for accurate performance estimates. Alongside cars and trucks, smaller vehicles such as scooters and bicycles are also set to participate in V2X networking, but have received considerably less attention. In this work, we present an extensive characterization of the gain pattern of a bicycle and antenna system for the IEEE 802.11g standard. We measure the radiation patterns of the antenna of a commodity 2.4 GHz WiFi module mounted on six distinct positions on the body of six archetypal bicycles in an anechoic chamber. The RSSI sample set per angle and antenna position is characterized statistically and input into an empirical model of the gain pattern of the bicycle-antenna system. We define a bicycle-to-X propagation model that pairs the proposed bicycle-antenna gain and a log-distance shadowing path loss model, and conduct outdoor measurement campaign for evaluation. We observe that the gain model measured in chamber matches the measured RSSI at small distances, whereas at larger distances it provides less accuracy.

Characterization and Modeling of the Bicycle-Antenna System for the 2.4GHz ISM Band

Luís Pinto and Pedro M. Santos*
Universidade do Porto
Portugal
{lpinto,pmsantos}@fe.up.pt

Luís Almeida
Universidade do Porto
CISTER
Portugal
lda@fe.up.pt

Ana Aguiar
Universidade do Porto
Instituto de Telecomunicações
Portugal
anaa@fe.up.pt

***Abstract*—Vehicular communication is rapidly becoming a standard reality, and precise models are necessary for accurate performance estimates. Alongside cars and trucks, smaller vehicles such as scooters and bicycles are also set to participate in V2X networking, but have received considerably less attention. In this work, we present an extensive characterization of the gain pattern of a bicycle and antenna system for the IEEE 802.11g standard. We measure the radiation patterns of the antenna of a commodity 2.4 GHz WiFi module mounted on six distinct positions on the body of six archetypal bicycles in an anechoic chamber. The RSSI sample set per angle and antenna position is characterized statistically and input into an empirical model of the gain pattern of the bicycle-antenna system. We define a bicycle-to-X propagation model that pairs the proposed bicycle-antenna gain and a log-distance shadowing path loss model, and conduct outdoor measurement campaign for evaluation. We observe that the gain model measured in chamber matches the measured RSSI at small distances, whereas at larger distances it provides less accuracy.**

***Index Terms*—vehicular, antenna, bicycle, radiation pattern, device-to-device channels**

I. Introduction

Bicycles are a widely used commute solution [1] but, from a safety standpoint, cyclists are deemed Vulnerable Road Users (VRU) given their inferior protection levels. Bicycle-to-bicycle links (Bi2Bi), and links between bicycles and other road users or infrastructure (Bi2X) may support safety applications via low-latency direct communication, thus protecting the life of cyclists and other road users [2]. Such networking may also support infotainment applications that improve cyclists' mobility experience altogether. Yet, there are no comprehensive studies on the shadowing or reinforcement induced by a bicycle frame on the wireless signal transmitted by an on-board antenna. Existing works study the shadowing caused by cars and scooters for the purpose of characterizing them as obstacles or inform antenna placement [3]–[5], but similar studies and generic models of signal shadowing/reinforcement for bicycles are scarce or non-existent. We argue that the signal transmitted or received by an antenna installed on a bicycle is shadowed or reinforced by the bicycle body; thus, we model the impact of the two elements on the wireless signal as the gain of a single transmitter/receiver body: the bicycle-antenna system (or B-A system).

*The two authors contributed in equal measure to the article.

In this paper, we present an extensive characterization of the gain of the bicycle-antenna system and propose an empirical model for this gain. The gain of the bicycle-antenna system $G_{\text{B-A}}$ is defined with respect to the gain of the bare antenna and modelled as a deterministic function of the angle and antenna position. The gain model can be incorporated in existing propagation models such as the log-distance shadowed path-loss model. We perform measurements in an anechoic chamber to characterize the gain of the bicycle-antenna system and inform the model design, and carry out outdoor measurements with bicycles in motion to evaluate the model. We focus on a widely available commercial wireless technology, namely WiFi (IEEE 802.11b/g), operating on the 2.4 GHz ISM band.

Our contributions are the following:

- Characterization of the gain patterns of the archetypal bicycle, with six different antenna positions;
- A generic model of the gain of a bicycle-on-board antenna system, as a function of angle and antenna position;
- Performance evaluation of the proposed gain model against measurements in an outdoor dynamic scenario.

To the best of our knowledge, no related work provides such characterization of the bicycle impact on the signal of an on-board antenna, nor evaluates its accuracy in a real-world test.

The remainder of this article is structured as follows. Section II is dedicated to a literature revision on vehicular propagation studies. Section III presents the gain model framework. An experimental campaign to characterize the gain of the bicycle-antenna system are reported in Section IV. The proposed model is evaluated in Section V. Conclusions are drawn in Section VI.

II. Related Work

A number of works study signal reinforcement or attenuation by vehicles in two contexts: a) vehicle passes between wireless terminals (i.e., it is considered an obstacle); b) antenna is installed in the vehicle. Regarding the first context, the work in [6] studies the impact of vehicles as obstacles in the received signal strength (RSS/RSSI) and assesses the packet delivery ratio of vehicular line-of-sight (LoS) and non-LoS channels for a range of distances. The authors measure obstruction by a van, a truck, reporting drops in RSS of 20 and 27 dB respectively, and observing that attenuation

978-1-5386-9428-2/18/$31.00 ©2018 IEEE

decreases as distance between terminals increases. In general traffic, the authors compare the experimental RSS samples with the double-edge knife (DKE) model [7], concluding that the DKE model over-estimates RSS due to not accounting for environmental factors. The authors of [8] perform a similar and more recent analysis, focusing specifically on the shadowing by vehicles and reporting this to follow a normal distribution with mean varying between 3.38 dB to 9.33 dB (depending on scenario and vehicles). The authors of [4] also characterize the attenuation of vehicles of different types. Using two cars with antennas on the rooftop in highway environment, they measure the path loss in line-of-sight and with inter-positioned vehicles namely a car, a van and a truck. In [9], the authors deployed two antennas at the sides of a road and measured the attenuation of several road-users and vehicles as they interfere with the on-going link. In the second study context (antenna on vehicle), the work reported in [10] characterizes the influence of a car body on the 3D radiation pattern of an antenna installed on the left rear-view mirror by means of simulation. The authors report that signal reinforcement up to 5 dB can be expected in some angles. In [3], the authors study several positions for an antenna in the rooftop of a private vehicle. They collect radiation patterns for each position concluding that the front driver location is the most suitable. The work in [5] is possibly the closest to ours, as it deals with scooters. The authors measure received signal strength from antennas positioned in several locations and study vehicle shadowing for the purpose of informing antenna positioning specifically for same-direction communication.

Literature on the attenuation of the human body in the wireless signal can be binned into the same two contexts: a) human passes between wireless terminal [11]–[13]; b) wireless device is close to human (e.g., smart phone) [14]–[16]. The works in [12] and [13] fit the first category. They measure human shadowing in the 2.4 GHz band in indoor scenarios, reporting respectively a drop of 17 dB for slow-walking interfering humans, and signal shadowing of 20 dB and reinforcement of up to 9 dB. In [5], the authors report a drop in 10 dB caused by the passenger.

To the best of our knowledge, no other work has explored bicycle-induced signal shadowing and/or reinforcement for on-board antennas. We also argue that existing literature on cars and scooters cannot be directly applied. Cars are covered by large sheets of (typically) reflective metal, and the consensual location to place an antenna for vehicular-to-X applications, the rooftop (due to its unobstructed isotropic view), is not available on bicycles. Scooters, as bicycles, do not have a passenger cabin and most of the exposed material is structural, but there are more metal surfaces (e.g., protective panels for scooter front and engine bay), electromagnetic noise (from the engine), the frame may be shaped differently (as the rider does not need to pedal), and some elements do not occur in both types of vehicles (e.g., pedals, rear-view mirrors). Antenna placement in scooters is also not straightforward, and/or may depend on the target application.

III. Bicycle-Antenna System Gain Model

We present now an empirical model of the gain that a bicycle-antenna system (B-A system) can cause on a wireless signal, with the purpose of modelling the performance of bicycle-to-anything (Bi2X) links.

The standard free-space propagation model (based on the Friis transmission equation) describes the received signal strength P_{rx} as the sum (in the logarithmic domain) of the transmit power P_{tx}, the free-space path-loss attenuation L_{lp}, and the gains of the transmitter and receiver systems $G_{\text{B-A (tx)}}$, $G_{\text{B-A (rx)}}$ (among other elements). Empirical models such as the log-distance shadowing path-loss model (LDSP model) [17] extend the free-space formulation by defining a scenario-specific attenuation rate α and including a stochastic component that captures the variability inherent to wireless measurements (slow fading). This stochastic component is typically modeled as a normally-distributed random variable X_σ with zero-mean and standard deviation σ. The resulting propagation formula is shown next.

$$P_{\text{rx}}[\text{dBm}] = P_{\text{tx}} + G_{\text{B-A (tx)}} + G_{\text{B-A (rx)}} + L_{\text{pl}} + X_\sigma \quad (1)$$

When estimating the parameters of an empirical model (such as the LDSP), P_{tx} can be replaced by the received signal strength P_0 at a known distance d_0, and L_{pl} can be described by

$$L_{\text{pl}} = 10\,\alpha\,\log_{10}\left(\frac{d}{d_0}\right) \quad (2)$$

where α is the scenario-specific attenuation rate.

In this work, we propose empirical models for the two remaining parcels of the Eq. 1, $G_{\text{B-A (Tx)}}$ and $G_{\text{B-A (Rx)}}$, for the case of a Bi2Bi communication scenario (or a Bi2X scenario, if only one bicycle is involved). The resulting model, an adapted version of the LDSP model, is refered to as bicycle-antenna system log-normal shadowing path-loss model (BAS-LDSP model).

A. Gain Model

The proposed gain model is defined in the fashion of a gain pattern, i.e., signal gain as a function of the angle between the bicycle heading and the straight line to the other bicycle – or line-of-sight (LoS) angle. The LoS angle is variable and the gain at such angle may vary with relevant design variables such as: antenna position (e.g., handlebar, under-seat) and orientation (e.g., vertical or tilted w.r.t. horizontal plane), bicycle frame format (e.g., diamond, step-through) and frame material (e.g., steel, aluminum).

The first three variables are critical in defining the section of bicycle body that an electromagnetic ray at a certain angle crosses or is exposed to, whereas the latter (frame material) may cause a larger or smaller intensity in the signal attenuation/reinforcement. In practice, in the measurement campaign we carried out in an anechoic chamber, we observed experimentally that the bicycle frame material exhibits little impact on the B-A system gain. The frame format was not studied in detail and, regarding antenna orientation, we focus

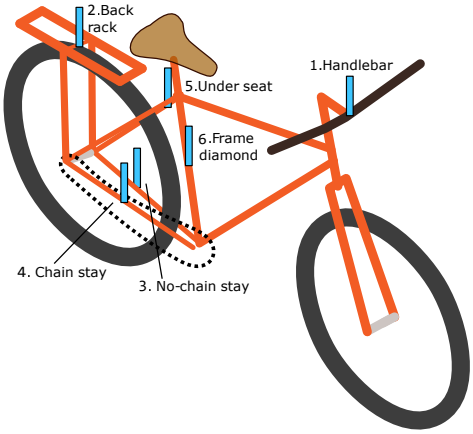

Fig. 1: Six positions for antenna placement (p): Handlebar (1), Back-rack (2), No-chain stay (3), Chain-stay (4), Under-seat (5), Frame diamond (6).

(A) diamond, steel frame. (B) diamond, aluminum frame. (C) narrow diamond, aluminum frame.

(D) hybrid, steel frame. (E) step-through, aluminum frame. (F) diamond, steel frame.

Fig. 2: Six bicycles were used for the experiments; all had back racks installed.

on dipole antennas propagating isotropically in the horizontal plane. Thus, we define the proposed empirical model of the bicycle-antenna system gain $G_{\text{B-A}}$ as a function of:

- Angle of the bicycle heading to the remote terminal – θ;
- Position of antenna in the bicycle – p.

The value of $G_{\text{B-A}}$ per angle (and position) is decomposed in a deterministic and a stochastic component. The deterministic component K is the average transmit power of a B-A system. The random variable ξ captures the variations intrinsic to wireless signal measurements (i.e., measurement error); we consider its mean to be 0 (i.e., it is centered around the value of the deterministic component). Formally, it can be written as:

$$G_{\text{B-A}}(\theta, p) = K(\theta, p) + \xi \tag{3}$$

A dedicated measurement campaign (such as that of Section IV) provides values for K for a discrete set of angles and positions (that can be implemented as a look-up table).

B. Selected Antenna Positions

We selected a set of six antenna positions that minimally disturb the rider, allow the antennas to be robustly strapped to the chassis, and are typical and/or viable points to install support equipment by system designers. The positions are shown in Figure 1, and their advantages and shortcomings (in particular for isotropic propagation in the horizontal plane) are discussed next.

Pos. 1 **Handlebar**: the center of handlebar is the most common location for placing cycling-support gadgets, such as smart phones and performance meters. From an antenna perspective, this location offers little shadowing as few bicycle elements are at the same height.

Pos. 2 **Back-rack**: many bicycles feature a back or front rack for carrying additional loads. From a propagation stand-point, its far-end offers unimpeded EM propagation towards the back and sides of the bicycle.

Pos. 3 **No-chain stay**: the bar between the axes of the back wheel and of the pedals, on the side opposite to the chain, provides an unimpeded, horizontal volume where an embedded device can be installed. The antenna is close to moving objects (e.g., legs, wheels).

Pos. 4 **Chain-stay**: similar to the previous position, but on the chain side. In this case, the antenna is also close to the chain system (i.e., chain, crankset and cogset). This position is motivated from a product design perspective, as numerous commercial products use the space within the chain to store embedded electronics, e.g., batteries, dynamos, communication devices (often within a protective encasing).

Pos. 5 **Under-seat**: support gadgets or pockets are sometimes installed under the seat. It is an open and reasonably protected space, and is not close to objects performing large movements.

Pos. 6 **Frame diamond**: the interior of the frame diamond is used very often to place support objects (e.g., water bottles and pouches). However, it is a region around which there is considerable leg movement and the shadowing may be substantial.

IV. Experimental Parametrization

We present the methodology of the radiation pattern measurements carried out to identify the relevant variables, populate the parameters of the B-A system gain model, and provide an analysis of the results.

A. Equipment and Methodology

We designed the experiments to explore the variables that we hypothesized that could affect the gain of the bicycle-antenna system, specifically antenna position and frame material. Antenna orientation and frame format were not evaluated.

We carried out radiation pattern measurements on six different bicycles, shown in Figure 2. Three of these bicycles have

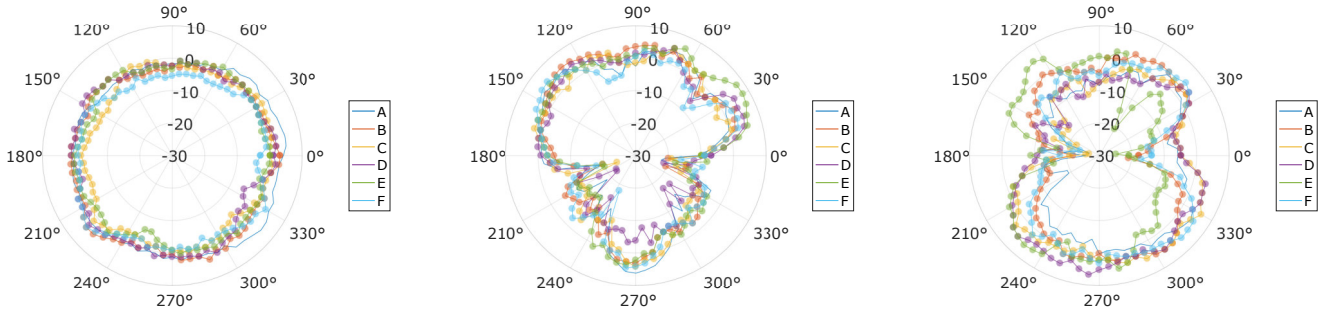

(a) Handlebar position (b) No-chain stay position (c) Frame diamond position

Fig. 3: Gain patterns of all six bicycles per angle, for 3 representative positions. Angle represents bicycle heading w.r.t. TX antenna (0º means bicycle points to TX antenna; 90º means the bicycle's right side is facing the TX antenna).

a frame of steel and three have a frame of aluminum, with the purpose of studying the impact of material. Their formats vary slightly: three have an ordinary diamond-shaped frame, one has a narrow diamond frame, one has a step-through frame, and one has a hybrid frame (step-through and narrow diamond). The wireless modules used in the measurements were the IEEE 802.11g-compliant TP-LINK TL-WL722N, that are equipped with a 4dB dipole antenna.

The measurements were done in a 6m-by-3m anechoic chamber equipped with a turn table. The bicycles were placed one at a time on the table, and equipped with the wireless modules installed in the six positions discussed in Section III-B. Another wireless module was placed in a pole located 4.26m away. All modules were connected via USB cables to PCs on the exterior of the chamber. The TX module transmitted WiFi ad-hoc beacons every 100ms, at a standard 1Mbit/s and 0.1W of power. The RSS at the RX module was collected in the PC using *tcpdump*. The PCs were running Ubuntu 16.04 kernel 14.13 x64. Bicycles performed a full revolution, stopping for 20 seconds every 5º to collect RSS samples. The rotation axis was aligned with the geometrical center of the bicycle. The distance offset that antennas had to the bicycle center (and that varies with bicycle heading) was accounted for in the presented gain results.

For reference/control purposes, we measured the gain of a bare antenna using a similar WiFi module with the same 5º resolution. The resulting pattern showed an expected isotropic behavior and collected RSS samples presented a normal distribution, with a global average P_{ref} of -35.8 dBm and a standard deviation σ_{ref} of 0.75 dB. The global RSS average of this measurement was used as a reference RSS P_{ref} for all subsequent RSS measurements, i.e., we remove P_{ref} to obtain the gain of the B-A system for each antenna position and angle. In some conditions, we observe signal reinforcement.

B. Statistical Analysis Towards a General Gain Model

In Figure 3, we present the measured gain patterns for all bicycles (overlapped) for three representative positions, namely handlebar, no-chain stay, and frame diamond. These diagrams show differences in the bicycle-antenna system gain when different antenna positions are used and that, for the same position, the pattern shape is consistent across various bicycles. The latter empirical observation motivates the proposed approach of characterizing the per-angle gain with statistical parameters (mean and deviation), as in Eq. 3.

Figure 4 shows the average gain patterns for the six bicycles. The colors provide visual cues of different levels of gain: same gain as bare antenna (yellow); positive gain w.r.t. to bare antenna (green); and attenuation w.r.t. bare antenna (red). We define same gain as bare antenna if the average bicycle gain for that angle is within a margin of ± 1.5 dB. This value corresponds to $2\sigma_{\text{ref}}$ – two reference standard deviations of the bare antenna samples. On the right of each gain diagram, a histogram shows the distribution of measured gain for each class (centered on the mean of that class). As a general rule, the distributions of samples with positive gain (green) and null gain (yellow; when sufficient samples are available) seem to follow a normal distribution.

We make the following remarks about the B-A system gain pattern for each antenna position:

Pos. 1 **Handlebar**: provides almost null and isotropic gain, as it is exposed to little surrouding material.

Pos. 2 **Back-rack**: exhibits positive isotropic gain, with just a minor attenuation towards the front due to the frame.

Pos. 3 **No-chain stay**: major attenuation towards the right side of the bicycle (as the antenna is installed on the left side), although a positive gain can be observed in a subset of angles. The left side shows positive gain.

Pos. 4 **Chain-stay**: symmetrical to the previous case.

Pos. 5 **Under-seat**: provides near isotropic radiation except for a noticeable attenuation towards the front of the bicycle, due to shadowing by the bicycle frame.

Pos. 6 **Frame diamond**: highly attenuated along the longitudinal axis and nearly unimpaired gain on the sides.

Figure 5 depicts the measured gain samples per bicycle and their standard deviation, and the deviation of the bicycle mean to the global mean. For all positions, bicycles are presented in order to form two clusters: columns 1 to 3 refer to steel-frame bicycles (A, D, F), and columns 4 to 6 to aluminum-frame bicycles (B, C, E). The average mean deviation per

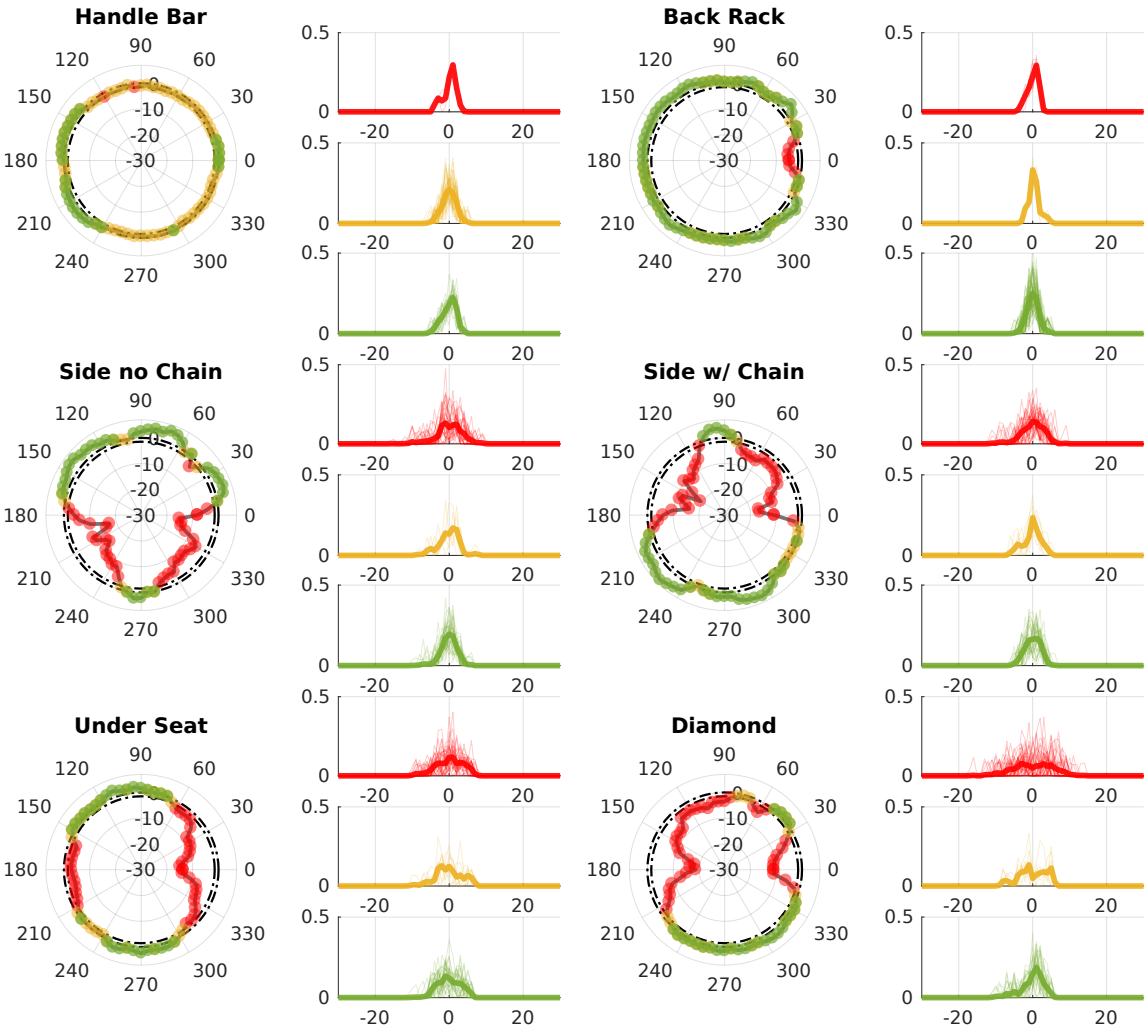

Fig. 4: For each antenna position: left - radiation pattern indicating the average B-A system gain per angle, relative to the reference, which can be positive (green), between 1.5 and -1.5dB (yellow), or below -1.5dB (red); right - distribution of gain deviation from average for all angles in the corresponding three sets.

clusters is also presented (up and down gray triangles). Several observations can be drawn. Antenna positions with great amount of surrounding material (e.g., under-seat, chain-stays and frame diamond), tend to have larger deviations among different bicycles. This confirms that less isotropic bicycle-antenna system radiation patterns are more dependent on the particular bicycle being used. Also, the material of the bicycle frame has little impact on the measured gain of the bicycle-antenna system. The mean deviation per cluster (shown by the triangles) does not allow to conclude about significant differences between steel and aluminum bicycles.

C. Conclusion and Practical Takeaways

The main factor defining the gain patterns are signal obstruction by the bicycle body. As could be expected, antenna positions along the longitudinal axis of the bicycle show symmetric gain patterns, whereas side-bound positions exhibit more or less elaborate gain patterns that reflect LoS opportunities on some angle windows (namely, the chain stay positions). Positive gain with respect to a bare antenna, never above 10 dBs, was observed in most positions. The frame material did not show statistical evidence of being a relevant factor in the overall gain patterns.

V. Model Evaluation in Dynamic Bi2Bi Scenarios

We evaluate the proposed gain model, incorporated in the BAS-LDSP model (Eq. 3), by producing RSS estimates and comparing these against field measurements. The field measurements address dynamic scenarios of bicycle-to-bicycle communication (one bicycle moving and with passenger).

A. Outdoor Bi2Bi Experiments

The following experiment replicates a Bi2Bi communication scenario involving two bicycles equipped with wireless modules. All experiments were carried out in a standard-size soccer pitch (100x64m). One of the bicycles was left standing at 12.5 meters of the pitch limit, aligned with the half-way line, for the entirety of the experiments and with no passenger.

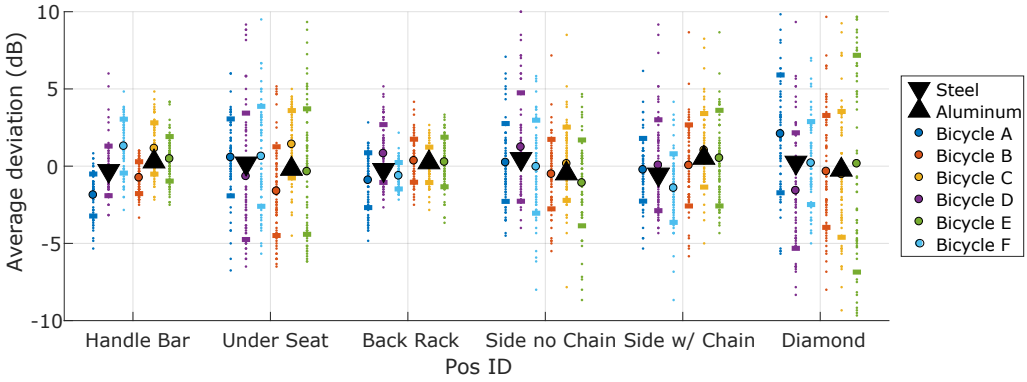

Fig. 5: Per-bicycle samples and standard deviation to bicycle mean, and deviation of per-bicycle mean to global mean. Per bicycle, black-bordered circles indicate deviation from global mean and bars indicate standard deviation. Per position, first three columns refer to steel-frame, remaining to aluminum; triangles indicate cluster's average deviation.

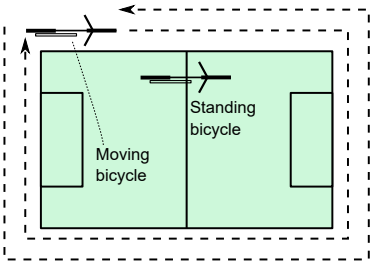

Fig. 6: RSS measurements were divided into two campaigns (two different antenna positions); each had two sessions (CW and CCW motion). Outside bicycle marks starting position.

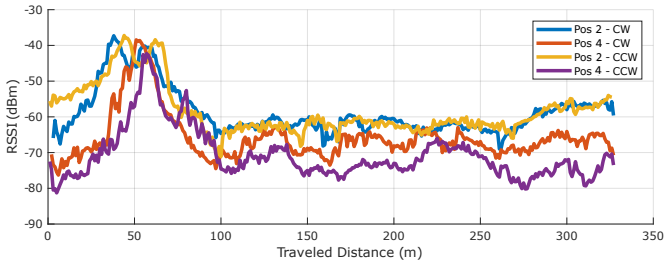

Fig. 7: Time-series of measured RSS in the four measurements sessions. Shown values are average of three trips for available distances and interpolated where samples are missing.

The other bicycle, carrying a cyclist, performed three trips around the pitch per session. This particular arrangement and trajectory configuration was selected because it covers a large range of distances and almost the entirety of angles between the two bicycles. The full experiment was composed of four measurement sessions, differing in antenna position and direction. In two sessions, the back-rack position was used, as it presents a simple gain pattern and thus it is easier to interpret collected results, and in the other two sessions the chain-stay position was used, as a location that features considerable variations in gain and attenuation. The two sessions per antenna position differed in the direction around the field – clockwise (CW) and counter-clockwise (CCW). Note that, in the case of the chain-stay position, in one travel direction (CW) the antenna is facing inwards to the pitch, and in the other direction (CCW) is facing outwards the pitch. Figure 6 depicts the performed trajectory, with the moving bicycle marking the starting position.

In the field measurements, two bicycles were equipped with a communication setup similar to that of Section IV-A: a TP-Link WL722N module connected to a PC installed in the back rack of the bicycle. RSS samples were collected using *tcpdump*. The bicycle position was recorded using GPS receivers (BU-232 USB GPS). The results for all four sessions are shown in Figure 7, averaged over the three trips per session. We observe that the measured RSSI profile is similar for both directions of the antenna in the back-rack, as expected, since the radiation pattern is the most isotropic. On the other hand, the differences in measured RSSI between the two sessions for the chain-stay position is more significant, and the RSS is lower on average.

B. Model Usage and Evaluation

The RSS estimates $\hat{\rho}$ can be computed from the BAS-LDSP model depicted in Eq. 1: $P_{\text{rx}} = P_{\text{tx}} + G_{\text{B-A (Tx)}} + G_{\text{B-A (Rx)}} + L_{\text{pl}} + X_{\sigma}$. The parcels $G_{\text{B-A}}$ refer to the bicycle-antenna system gain model presented in the previous sections. The parameters of the log-normal shadowing path-loss model P_{LDSP} were drawn from a dedicated measurement campaign. The resulting formula was $P_{\text{LDSP}}(d) = -21.376 - 21.39 \log_{10}(d) + X_{\sigma}$, where $X \sim \mathcal{N}(0, 0.548)$. This dataset was compared to the (non-empirical) two-ray ground model [17], and we observed a good fit (RMSE=4.1983 dB, vs. RMSE=3.1794 dB of LDSP model). For informative purposes, the turnover distance of the two-ray ground model, with transmitter and receiver at a height of 0.7m (for back-rack antenna position), is ∼15m (note that the minimum distance between bicycles, during the measurements, was 12.5m). The cyclist-induced shadowing was evaluated in dedicated radiation pattern measurements of the bicycle-antenna system with and without cyclist, using the back-rack position and in static conditions. We observed a drop of ∼10 dB when the cyclist torso is between the on-board and the probe antenna, a drop of 5 dB if the arm is in-between, and negligible contribution elsewhere. It is indicated

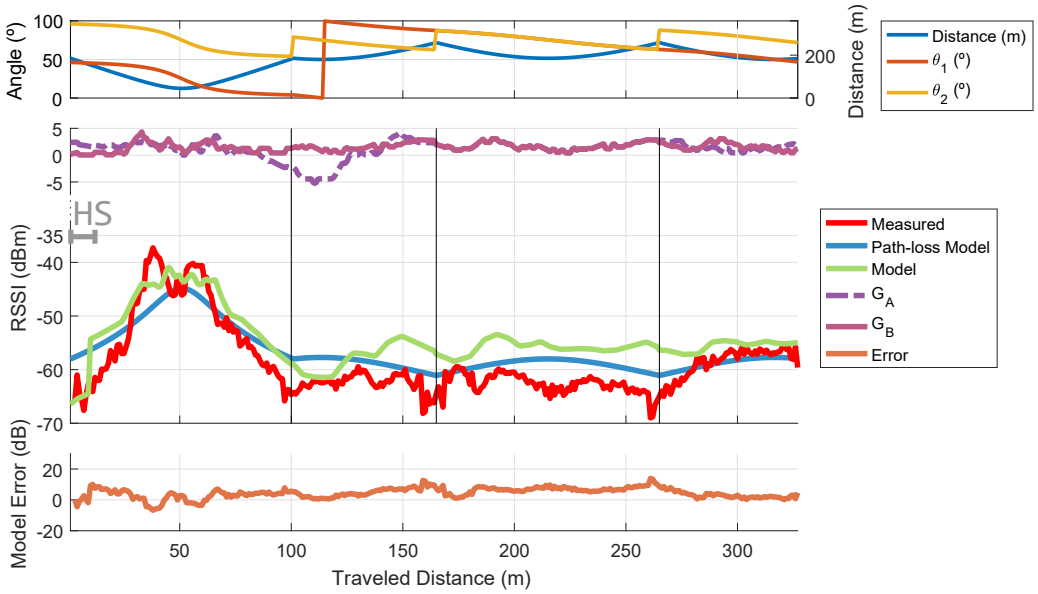

Fig. 8: Representative measurement session (position: back-rack; direction: CW) shown versus travelled distance around the field; black vertical lines mark field corners. Top: distances and bicycle orientations as circuit is performed. Center: time-series of measured RSS (red), modelled RSS (green), path loss (blue) and gains of both B-A systems (purple lines). Period of relevant human shadowing is shown by "HS" ruler and drop in "Model" line. Bottom: error between measured samples and estimates.

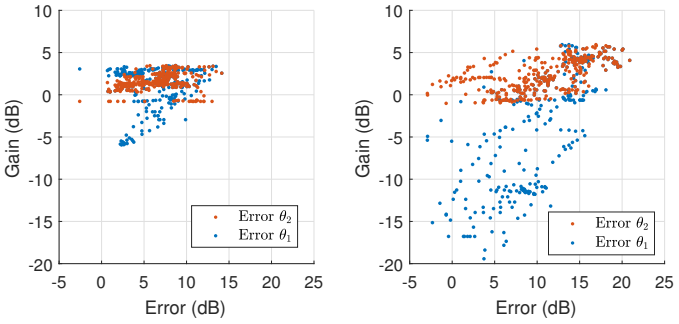

(a) Position back-rack. (b) Position chain-side.

Fig. 9: Pairs of model error and bicycle-antenna system gain values, paired by common angle of LoS (CW sessions only). No correlation between error, gain and angle is observed.

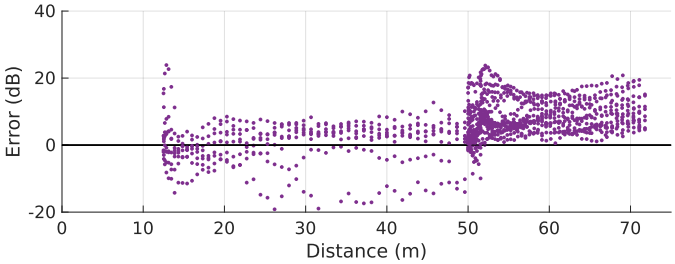

Fig. 10: Model error vs. distance between bicycles for all sessions (back-rack and chain-stay positions; CW/CCW).

in Figure 8 by a ruler on the leftmost side. The computation of RSS estimates $\hat{\rho}$ for a dynamic scenario was computed based on the distances and angles associated with each measured RSS sample ρ. Figure 8 shows the time series of measured RSS samples ρ and model RSS estimates $\hat{\rho}$ for a representative experimental session.

An important observation stemming from Figure 8 is that a large fraction of estimates $\hat{\rho}$ of the BAS-LDSP model are higher than the measured RSS ρ, for both positions. From visual inspection, we observe that the over-estimation takes place between the 120m and the 275m distances. We investigate the source of this behaviour by evaluating if the model error has a direct relationship with: a) particular angles and the gain patterns measured in chamber; b) particular distances between bicycles. In the first case, we search for a relation between the model error values at a given LoS angle and the bicycle-antenna system gain with the same radiation angle (to understand, e.g., if higher errors are related to higher gains). The corresponding pairs of model error and B-A system gain, for both transmitter and receiver bicycles (θ_1 and θ_2), and for both antenna positions (CW sessions only), are shown in Figure 9. We do not identify, by visual inspection, an obvious mathematical relation (linear, polynomial, etc.) between the model error and the B-A system gain for the corresponding angle, and thus cannot attribute the over-estimation behaviour to particular gain patterns. The second hypothesis is evaluated by plotting the model error versus the corresponding distance, as presented in Figure 10 for all sessions. Note that, due to the route that we followed, there is a large concentration of samples farther than 50 meters. For these points, the model notably over-estimates the RSS and produces few under-estimates: the mean of these error values is 7.95 dB and the standard deviation is 5.37 dB (universe of 916 samples). For distances below 50 meters, the model exhibits good performance: the mean and standard deviation of the error is 0.53 dB and 6.77 dB respectively (for 388 samples).

C. Discussion

Based on the observation that over-estimates occur mostly at larger distances, we put forward two hypotheses to justify the performance of the proposed model at those distances:

1) the gain patterns are impaired by phenomena not captured in the anechoic chamber;
2) the path loss component of the model does not describe accurately RSSI behaviour.

At large distances, the constructive interference that caused signal reinforcement of the bicycle-antenna system for some angles in the anechoic chamber may not occur at the same scale in an outdoor scenario. This can be attributed to the unaccounted factor that the measurements in the anechoic chamber may have taken place in the near field of the radiating system. In the near-field, reflected rays interfere in a way that is not representative of the gain that the radiating system presents in the far field. The outdoor experiments, taken at large distances and thus falling in the far-field, show indication that the chamber measurements are exhibiting such near-field gains. The second hypothesis is motivated by the empirical observation that, in the data collected in the campaign carried out to retrieve the path-loss model parameters, RSSI samples at larger distances experience more variability than at small distances.

VI. Conclusions and Future Work

We propose an empirical model of the gain of the bicycle-antenna system in the 2.4GHz band as a function of angle and antenna position. In order to simultaneously design the model (by identifying the most relevant characteristics) and populate its parameters, we measured the gain pattern of six bicycle-antenna systems in anechoic chamber and for six antenna positions. In antenna positions with large exposure to the bicycle body, we observe both signal reinforcement and attenuation, depending on the angle, with respect to the gain of a bare antenna. The frame material showed little impact in the overall pattern. Finally, we carried out an outdoor measurement campaign to evaluate the accuracy of the gain model, incorporated in an established empirical propagation model. We observed accurate estimates at small distances but a consistent over-estimation at larger distances, that we attribute to the unforeseen occurrence that anechoic chamber measurements may have been taken in the near-field of the radiating system, or to inaccuracy of the used path loss model.

In future work, we plan to test the first of the above hypotheses – that the measurements were taken in the near-field – by measuring the gain of the bicycle-antenna system at larger distances. If this is the case, future gain pattern measurements should take place in an anechoic chamber of adequate size for the bicycle-antenna system. Additional lines of work include applying the empirical model to scenarios with other types of vehicles (e.g., cars), and develop an alternative description of the measured data (e.g., statistical, data-based) that facilitates integration into major networking simulations tools (e.g., ns-3, OmNet++/INET).

Acknowledgments

The authors wish to thank M. Rosa, J. Pintor, J. Mesquita, D. Rodrigues, P.M.d'Orey, M. Coelho, C. Silva and H. M. Silva for the help with the measurements. This paper is a result of the project Generation.Mobi (POCI-01-0247-FEDER-017369), and was supported by project S2MovingCity (CMUPERI/TIC/0010/2014), project SmartCityMules (PTDC/EEI-TEL/2008/2014) and IT internal funds (UID/EEA/50008/2013), funded by the applicable framework: European Regional Development Fund (ERDF), through COMPETE 2020, FCT/MEC (PIDDAC).

References

[1] E. Commission, "Quality of transport report," 2016.
[2] "The self-driving car's bicycle problem," 2016.
[3] S. Kaul, K. Ramachandran, P. Shankar, S. Oh, M. Gruteser, I. Seskar, and T. Nadeem, "Effect of antenna placement and diversity on vehicular network communications," in *4th Annual IEEE Communications Society Conference on Sensor, Mesh and Ad Hoc Communications and Networks*, June 2007, pp. 112–121.
[4] M. Segata, B. Bloessl, S. Joerer, C. Sommer, R. L. Cigno, and F. Dressler, "Short paper: Vehicle shadowing distribution depends on vehicle type: Results of an experimental study," in *2013 IEEE Vehicular Networking Conference*, Dec 2013, pp. 242–245.
[5] H.-M. Lin, H.-M. Tsai, and M. Boban, "Scooter-to-x communications: Antenna placement, human body shadowing, and channel modeling," *Ad Hoc Networks*, vol. 37, 09 2015.
[6] R. Meireles, M. Boban, P. Steenkiste, O. Tonguz, and J. Barros, "Experimental study on the impact of vehicular obstructions in vanets," in *IEEE Vehicular Networking Conf.*, Dec 2010, pp. 338–345.
[7] J. Kunisch and J. Pamp, "Ultra-wideband double vertical knife-edge model for obstruction of a ray by a person," in *2008 IEEE International Conference on Ultra-Wideband*, vol. 2, Sept 2008, pp. 17–20.
[8] Q. Wang, D. W. Matolak, and B. Ai, "Shadowing characterization for 5-ghz vehicle-to-vehicle channels," *IEEE Transactions on Vehicular Technology*, vol. 67, no. 3, pp. 1855–1866, March 2018.
[9] R. J. Weiler, M. Peter, W. Keusgen, K. Sakaguchi, and F. Undi, "Environment induced shadowing of urban millimeter-wave access links," *IEEE Wireless Comm. Lett.*, vol. 5, no. 4, pp. 440–443, Aug 2016.
[10] S. Imai, K. Taguchi, T. Kashiwa, and T. Kawamura, "Effects of car body on radiation pattern of car antenna mounted on side mirror for inter-vehicle communications," in *2014 IEEE Antennas and Propagation Society International Symposium (APSURSI)*, July 2014, pp. 601–602.
[11] M. Peter, M. Wisotzki, M. Raceala-Motoc, W. Keusgen, R. Felbecker, M. Jacob, S. Priebe, and T. Kürner, "Analyzing human body shadowing at 60 ghz: Systematic wideband mimo measurements and modeling approaches," in *2012 6th European Conference on Antennas and Propagation (EUCAP)*, March 2012, pp. 468–472.
[12] J. S. C. Turner, M. F. Ramli, L. M. Kamarudin, A. Zakaria, A. Y. M. Shakaff, D. L. Ndzi, C. M. Nor, N. Hassan, and S. M. Mamduh, "The study of human movement effect on signal strength for indoor wsn deployment," in *IEEE Conf. on Wireless Sensor*, Dec 2013, pp. 30–35.
[13] H. Hongwei, S. Wei, X. Youzhi, and Z. Hongke, "The effect of human activites on 2.4 ghz radio propagation at home environment," in *2009 2nd IEEE International Conference on Broadband Network Multimedia Technology*, Oct 2009, pp. 95–99.
[14] M. Ghaddar, L. Talbi, T. A. Denidni, and A. Sebak, "A conducting cylinder for modeling human body presence in indoor propagation channel," *IEEE Transactions on Antennas and Propagation*, vol. 55, no. 11, pp. 3099–3103, Nov 2007.
[15] S. L. Cotton, "Human body shadowing in cellular device-to-device communications: Channel modeling using the shadowed $\kappa - \mu$ fading model," *IEEE Journal on Selected Areas in Communications*, vol. 33, no. 1, pp. 111–119, Jan 2015.
[16] N. Fet, M. Handte, and P. J. Marrón, "A model for wlan signal attenuation of the human body," in *ACM International Joint Conference on Pervasive and Ubiquitous Computing*. ACM, 2013, pp. 499–508.
[17] T. Rappaport, *Wireless Communications: Principles and Practice*, 2nd ed. Upper Saddle River, NJ, USA: Prentice Hall PTR, 2001.